



What are the hygrothermal consequences of applying exterior air barriers in timber frame construction in Europe?

Keywords: HAM, air convection, numerical simulation, building component, exterior air barrier

Abstract

Moisture induced damage is one of the major causes of degradations and reduced thermal performance in wood frame buildings. It is therefore crucial to incorporate the hygrothermal assessment of new timber frame building envelopes systems from the early development phase onwards.

The article at hand presents the simulation results studying the hygrothermal performance of various timber frame wall configurations with exterior air barrier systems. A parameter analysis explores the impact of different European climates, insulation materials, exterior air barrier materials and bad workmanship in the installation of the insulation layer.

This study reveals that the application of mineral wool insulated timber frame walls in combination with exterior air barriers results in increased moisture loads. Moreover, small air channels between the mineral wool and the adjacent exterior air barrier significantly increase natural convection and add up to harmful moisture levels. Yet the simulations indicate that the use of blown-in cellulose insulation can avoid these issues. The study further indicates that the technique of exterior air barrier is more suitable for continental climates rather than for moderate sea climates in Europe.

Nomenclature		λ	Thermal conductivity	W/m/K
Abbreviations		μ	Water vapour resistance factor	-
BIFB	Bituminous impregnated fibreboard	Π_y	Drying potential:averaged difference between actual and v	kg/m ³
CL	Cellulose insulation	ρ	Mass density	kg/m ³
FCB	Fibre cement board	θ	Temperature	K
GB	Gypsum Board	Symbols		
MW	Mineral wool	c_p	Heat capacity	J/kg/K
OSB	Oriented Strand Board	AC_{max}	Maximum accumulated condensate	kg/m ²
Subscripts		G_{vp}	Vapour production	kg/s
	Parallel	d	Thickness	mm
⊥	Perpendicular	HIR*	Hygric inertia	kg/(m ³ %RH)
out	Outdoor	K	Air permeance	m ²
s	Surface	RH	Relative humidity	%
sat	Saturation	v	Humidity by volume	kg/m ³
Greek letters				

1 Introduction

Energy consumption and sustainability is a growing priority for house owners, so, particularly in the last decade, considerable progress has been made to improve the energy efficiency of buildings. Minimising unwanted air infiltration through the building envelope is one of the key elements to achieve energy efficient buildings (Jokisalo et al. 2009). As a consequence, several European member states recently increased their airtightness requirements. Moreover, labels to certify standardised low energy buildings, requiring very high airtightness standards, are increasingly established across Europe. For example the 'Passivhaus'-standard explicitly requires a building airtightness of 0.6 air changes per hour (ACH) at 50 Pa. Apart from improving energy efficiency, the second major motivation for creating airtight building envelopes is moisture control. Interstitial condensation in building enclosures is primarily the result of forced air exfiltration in winter conditions (Tenwolde & Rose 1996). According to Janssens (2003) condensation quantities related to exfiltration are typically two to three orders of magnitude higher than those transported by vapour diffusion.

For timber frame constructions an airtight building envelope is traditionally realised by an interior 'air barrier system', by sealing all the joints and intersections in the interior sheathing. In cold and moderate climates, such as North-West European areas, this air barrier function is often combined with that of the 'vapour retarder' (Janssens & Hens 2007, Thue et al. 1996). To protect the insulation layer from unwanted infiltration of outside cold air by natural or forced convection a 'wind barrier' is provided at the outside of the insulation (Janssens & Hens 2007). In addition, this exterior layer often serves as drainage plane to prevent water infiltration into the structure. The performance criteria for wind barrier systems regarding air permeance are less severe than for air barriers (Uvsløkk 1996). Therefore, the joints in the wind barrier are usually left unsealed.

Achieving the above mentioned high standards regarding global building airtightness with an interior barrier is labour-intensive. In installing an interior barrier a high number of difficult intersections, such as the connection between the intermediate floor and the outer walls, and perforations for electrical and plumbing services have to be sealed (Aho et al. 2008, Kalamees 2007). As a result, timber frame building industry is looking for cost-effective alternatives to meet the severe airtightness requirements. One of the possibilities is to realise the airtight layer at the outside of the building envelope where fewer joints are present. Recent studies show the advantage of improving the airtightness of the wind barrier, so, it will serve as an exterior air barrier system. In-situ measurements combined with laboratory tests show how minor modifications can significantly improve the air permeance of the wind barrier layer (Myhre & Aurlien 2005, Langmans et al. 2010, Holøs & Relander 2010). Focussing on the outer layer for the realisation of the building airtightness, and thus reducing the airtightness requirements of the inner vapour barrier may, however, significantly influence the hygrothermal behaviour of these elements in cold and moderate climates. In addition, when increasing the airtightness of the wind barrier, the airtightness level of the inner vapour barrier layer can no longer be evaluated individually. Quantifying the overall building airtightness with a pressurisation test will always correspond to a combination of both the airtightness of the interior and exterior layers. As consequence, it is important to investigate the hygrothermal performance of light-weight components with the most airtight layer at the outside of the building envelope. Laboratory measurements on full-scale test walls insulated with standard glass wool revealed that this technique might result in an increased moisture accumulation at the upper cold parts of the walls (Langmans et al.2012a). This is caused by buoyancy driven air rotations in the insulation layer, transporting humid interior air through imperfections in the interior vapour barrier towards the outer side of the insulation layer as depicted in Figure 1.

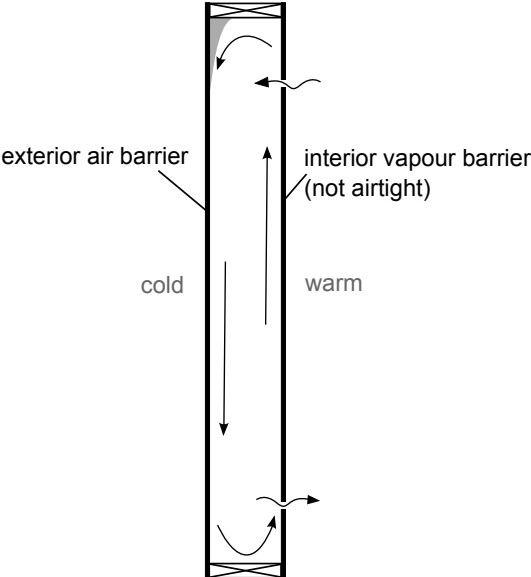


Figure 1: Moisture redistribution in a light-weight wall with an exterior air barrier (moisture accumulation in grey).

The above-mentioned laboratory work produced important insights in the physical phenomena of light weight walls with an exterior air barrier. Nevertheless, this experimental study is a significant simplification of reality in that the walls were exposed to constant (severe) winter climate conditions which may overestimate the moisture accumulation related to natural convection within the walls. Before the technique of exterior air barrier can be launched in practice, key question, however remains how these systems perform in real climate conditions.

The present paper performs heat, air and moisture (HAM)-simulations on light weight walls with exterior air barrier systems to explore the hygrothermal risks involved. Yearly simulations under realistic climate conditions were conducted with a state-of-art numerical model, capable to model forced and natural convection in interaction with detailed heat and moisture transport (Nicolai (2007), Langmans et al.2012b). The model applies a two-domain approach; (1) porous building materials with (2) adjacent air channels assuming fully-developed laminar flow. The current article performs numerical simulations to investigate the hygric response of exterior air barrier systems in timber frame construction. The main interest lies in the impact of (1) different insulation materials and (2) various exterior air barrier materials, (3) bad workmanship and (4) different European climate conditions.

2 Methodology

2.1 Numerical HAM-model

The HAM-model used in the present study is a modified version of DELPHIN 5, originally developed at the Technical University of Dresden. The governing and transport equations regarding heat, air and moisture transport in porous building components solved by this state-of-the-art simulation tool as well as the applied numerical strategy are described in detail in (Grunewald 1997, Nicolai 2007, Langmans et al. 2013).

The combined heat and moisture transport of this model has extensively been validated in the framework of the EU-initiated HAMSTAD (Heat, Air and Moisture Standards Development) project (Hagentoft 2002, Li et al. 2009, Tariku et al. 2010). In this project the model has been compared with other numerical HAM-models, showing good agreement. In addition, Langmans et al.2012b confronted this simulation tool to analytical (Weber 1975, Bories 1987), numerical (Janssens 1998, Saeid & Pop 2004) and laboratory (Langmans et al.2012) results from the literature to evaluate the interaction of air convection on heat and moisture transport in light weight components. The comparison with analytical and numerical models provided very good agreements. The confrontation with laboratory measurements, however, indicated larger deviations. Further investigations (Langmans 2013) on this topic revealed that this was mainly related to uncertainties in (1) the material properties and (2) the component configuration. The latter corresponds to small air channels within the building components amplifying the effects of buoyant driven air flows. Simulating building components as perfectly interconnected porous elements neglect such effects, and thus, underestimates air convection within building components (Brown et al. 1993, Silberstein & Hens 1996).

To incorporate cracks and small air channels between material interfaces, which are inevitable in real building com-

ponents, the porous calculation domain was extended with air channels. Air channels are introduced as a hydraulic network, assuming fully-developed laminar flow between parallel plates. These so-called Hagen-Poiseuille conditions are of course a simplification of reality. However, as air leakages in building components are unintended and can only be estimated roughly, it can be stated that this linearised approach is sufficient to evaluate the impact of air leakages on the hygrothermal behaviour of building components. This simplified method is used by various authors in the field of building physics such as [Lecompte \(1989\)](#), [Kronvall \(1980\)](#), [Hagentoft \(1991\)](#), [Kohonen \(1984\)](#), to describe combined heat and convection problems. The current implementation, applied for this study, is adopted from [Janssens \(1998\)](#) in which this methodology was extended with convective vapour transport in the numerical model 2DHAV. The implementation of this network approach in the framework of DELPHIN 5 and its confrontation with full-scale laboratory measurements is outlined in detail in [Langmans \(2013\)](#).

2.2 Wall configuration and discretisation grid

Figure 2a shows the general configuration applied in this study. This component corresponds to a typical timber framed wall applied in very low energy dwellings in Europe (e.g. Passivhaus-designs) and has an insulation thickness of 30 cm. Though, instead of a interior air barrier, the wall is provided with an exterior air barrier. Oriented strand board (OSB) is positioned on the inner side as interior vapour barrier. A service cavity of 40 mm is applied at the inside of the wall element, which is covered with a gypsum board finishing layer. Note that both the interior vapour barrier (OSB-layer) and this gypsum board layer are not continuously airtight, so, they will not act as an interior air barrier. Slots of 1 cm are provided at 20 cm from the top and bottom of the wall to simulate deficiencies in these interior layers. The air barrier, however, is positioned at the outer side of the insulation layer by assuming an continuously sealed exterior layer ([Langmans et al. 2010](#)). The walls are provided with a wooden cladding system at the outside with a ventilated cavity of 25 mm, containing top and bottom vents. In addition, Figure 2b illustrates the applied simulation grid which will be addressed in detail in section 4. The numerical model applies a control volume method for spatial discretisation of which the number of elements are indicated between brackets in this figure.

2.3 Material properties

This section outlines the hygrothermal properties of the applied materials. The most crucial properties within the simulations have been measured in the laboratory. The corresponding measuring protocols and detailed material properties are outlined in [Desta et al. \(2011\)](#) and [Langmans \(2013\)](#). This section only provides a brief overview of the applied material properties (see Table 1).

Untreated gypsum board (GB) is applied as interior finishing material. The corresponding material properties are adopted from [Roels et al. \(2010\)](#). Next, the vapour barrier consists of OSB panels at the inside. The wall is insulated with either mineral glass wool blankets (MW) or blown-in cellulose insulation (CL). Various kinds of exterior air

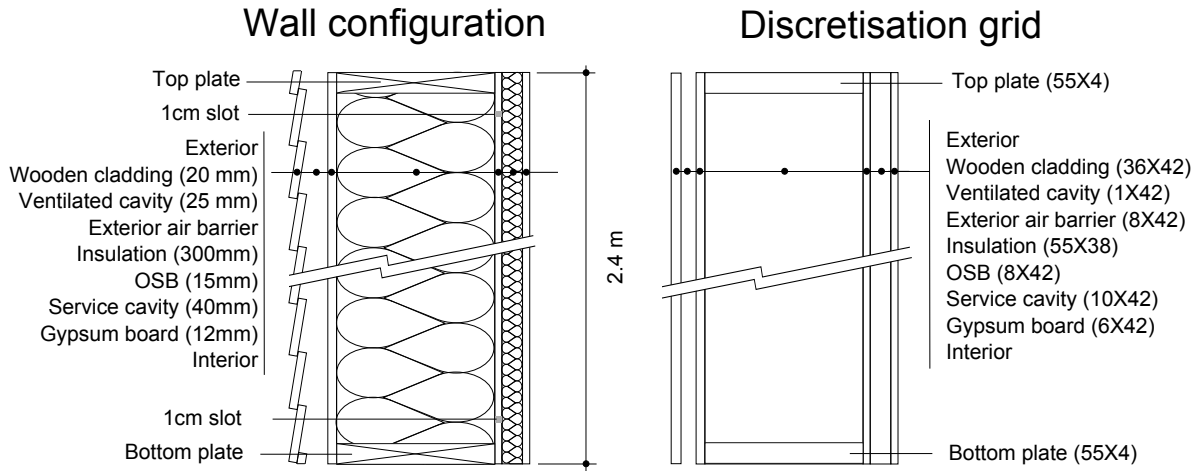


Figure 2: (a) Wall configuration and (b) corresponding simulation grid in which the number of elements are mentioned between brackets.

barrier are considered; (a) bituminous impregnated fibreboard with an additional air restive coating (BIFBa) and its variant without this coating (BIFBb), (b) fibre cement board (FCB), (c) spunbonded foils (FOIL), (d) gypsum board (GB) and (e) OSB. For the wooden top and bottom plates (see Figure 2) spruce is assumed. The properties of this material are based on the measurements of Zillig (2009). All simulation are provided with a wooden cladding system. The material properties of the cladding are based on Nore (2009); the wood cladding layer is modelled according to Zillig (2009) and its exterior paint layer has a constant water vapour diffusion thickness (μd) of 0.1 m.

	BIFBa	BIFBb	FOIL	OSB	MW20	CL60	spruce ^a	FCB	GB ^b
d (mm)	18	18	0.2	15	300	300	-	3	12
ρ (kg/m ³)	285	274	-	630	21.3	60	350	1400	690
c_p (J/kg/K)	2068	2068	-	1880	840	2544	1880	840	1090
λ_0 (W/m/K)	0.045	0.047	-	0.1	0.031	0.034	0.1	0.18	0.2
K_{\perp} (m ²)	$4.65 \cdot 10^{-13}$	$1.37 \cdot 10^{-11}$	airtight	$<8.20 \cdot 10^{-14}$	$8.1 \cdot 10^{-10}$	$8.8 \cdot 10^{-10}$	-	$<1.6 \cdot 10^{-14}$	$<6.6 \cdot 10^{-14}$
K_{\parallel} (m ²)	-	-	-	-	$5.3 \cdot 10^{-9}$	$3.2 \cdot 10^{-9}$	-	$<1.6 \cdot 10^{-14}$	$<6.6 \cdot 10^{-14}$
μ_{50} (-)	11.1	5.5	450	280	1	1.5	162	143	10
μ_{90} (-)	5.5	2.7	250	20	1	1.5	38	12	7.5

^aZillig (2009)

^bRoels et al. (2010)

Table 1: Overview of the material properties.

2.4 Evaluation method

Moisture performance limit states in timber frame building envelopes are often related to the onset of biological processes inside the component. These processes can imply bio-deterioration, which results in structural damage, and thus, shortens the buildings service life. In addition, surface mould formation may occur. This can be harmful to the inhabitants health and comfort, even without inducing structural damage. The majority of the existing moisture performance limit states are designed to prevent surface mould growth. The key parameters influencing this biological

process are humidity, temperature, exposure time and the exposed materials.

The literature puts forward two different methods to prevent biological activities in wood frame building enclosures: direct and indirect methods. The first approach consists of assessment methods that directly evaluate the main parameters inducing biological growth on organic materials (e.g. Sedlbauer 2001, Hukka & Viitanen 1999). The second method, on the other hand, assesses the level of interstitial condensation on (non)-organic materials, such as spun-bonded polyethylene foil (Janssens 1998). Here, the limit state corresponds to the onset of drainage which can result in accumulation of moisture, and thus, degradation of lower positioned wood based materials such as bottom plates.

2.4.1 Mould growth

The VTT-model (Hukka & Viitanen 1999) is applied for the evaluation of the mould growth in this study. This model is currently most recognised amongst the existing mould growth prediction methods in the international literature (e.g. Vinha 2007, Black 2006). The model is purely mathematical in nature and is based on linear regression analyses of laboratory data on mould growth in constant and transient conditions. As a consequence it is directly applicable as postprocessing tool, deriving the mould growth index from the temperature and relative humidity outputs. An extensive review on mould prediction methods by Vereecken & Roels (2012) showed, however, that induced by the various assumptions in these methods, large differences can be obtained. As a consequence it should be stressed that mould prediction tools are preferably used for comparing the mould growth risk of different components rather than making absolute predictions (Vinha 2007).

Mould spores are most obvious airborne components of fungal contamination, influencing occupant's health due to the settling and spreading of pathogens (e.g. Piecková & Jesenská 1996, Reboux et al. 2010). It remains, however, difficult to verify to which degree mould spores, located within the building envelope, influence the indoor air quality. Keeping in mind that this limit value will be treated more as a transition zone, a maximum mould growth level of 3 is applied in this work. This limit corresponds to a visual mould growth covering less than 10 % of the surface which seems to be reasonable for building materials located at the outside of the building envelope.

2.4.2 Interstitial condensation

When it comes to interstitial condensation, on the other hand, the moisture limit state should avoid run-off, and thus, moisture accumulation on lower regions within the building envelope. The onset of run-off caused by condensation is a complex phenomena depending for example on the materials surface roughness. As the detailed determination of these conditions, such as in Van den Brande et al. (2013), is beyond scope of the present simulations, a conservative simplified criteria is applied. The applied threshold value for condensation is adopted from Janssens (1998) who proposed a maximum value of 0.1 kg/m^2 . This limit is based on laboratory work on spunbonded foils. Such materials have a low surface roughness in comparison to the fibreboards applied in this study, so, the proposed limit state

corresponds to a conservative assumption.

3 Climate conditions

An important amount of uncertainties within hygrothermal simulations is related to the selection of representative weather data. In this context [Geving \(1997\)](#) defined a "Moisture Design Reference Year (MDRY) as the climatic data of the year corresponding to the highest hygrothermal stress on a construction component within a period of 10 year". However, the selection of a MDRY is a challenging process as the outcome of such an analysis highly depends on the building component studied, the envisaged limit state(s) and the simulation models complexity. [Janssens \(1998\)](#), for example, found that the exterior temperature is the most decisive parameter in selecting a MDRY for lightweight components, while [Geving \(1997\)](#) put forward the exterior relative humidity. This discrepancy can be explained by the fact that [Janssens \(1998\)](#) accounts for both diffusive and convective moisture transport while [Geving \(1997\)](#) only considered moisture transport by diffusion. Moreover, [Vinha \(2007\)](#) illustrated that the MDRY selection also depends on the applied moisture limit state criteria. [Vinha \(2007\)](#), who assessed the hygrothermal performance of a reference configuration for four different geographical locations in Finland and 30 consecutive years, showed that the MDRY for condensation conditions is not the most critical year for mould growth and vice versa.

In summary it can be stated that there is currently no consensus on reference climate data for hygrothermal building components simulations. Given its complexity, the selection of the most critical reference year to evaluate the performance of lightweight constructions lies beyond the scope of the present work. As a remedy, commonly available Test Reference Year (TRY) data from building energy simulations are used. The climatic data for this study is retrieved from the software package TRNSYS 17¹.

The walls are oriented to the North and hourly climate data is applied for the simulations within this study. The simulated air pressure difference across the wall is a combination of (1) stack pressure, (2) wind pressure and (3) mechanical ventilation. For the simulations at hand, the stack pressure is calculated for a two-storey building, assuming that the main leakages are located near the foundation, wind pressures are calculated based on surface-averaged pressure in which the wind pressure coefficients are adopted from [Swami & Chandra \(1987\)](#) and a 5 Pa overpressure is assigned for mechanical ventilation.

The inner temperature is assumed constant (20°C) throughout the year. Yet the inner humidity conditions are determined by a single zone model taking hygric buffering into account [Vereecken et al. \(2011\)](#):

$$\left(\frac{V}{R_v T_i} + \frac{100 HIR^* V}{p_{v,sat}(T_i)}\right) \frac{\partial p_{vi}}{\partial t} = (p_{ve} - p_{vi}) \frac{nV}{3600 R_v T_i} + G_{vp} \quad (1)$$

in which V (m³) corresponds to the volume of the room and HIR^* (kg/(m³ %RH)) to its hygric inertia, n (1/h) is the ventilation rate and G_{vp} (kg/s) is the vapour production in the room.

¹BE_UCCLE_64470

The parameters applied for the single zone model are chosen rather conservative: a small volume of 50 m³ with a high moisture load of two active persons (120 gram/h according to Hens (2010)) between 8h-22h. Based on the Belgian study of Stranger et al. (2012), in which actual ventilation rates were monitored, a ventilation rate of 0.5 l/h is applied in the simulations here. Finally, a value of 1.5 gram/(m³%RH) was assigned for the hygric inertia based on the measured values by Janssen & Roels (2009). The resulting interior humidity conditions are shown in Figure 3. Here, the vapour pressure difference between the interior and exterior conditions are compared to the humidity levels according to ISO 13788:2001. In addition to the conditions for a Belgium climate (Uccle), the resulting vapour pressure difference for Norwegian conditions (Oslo) are included in this figure (see section 3).

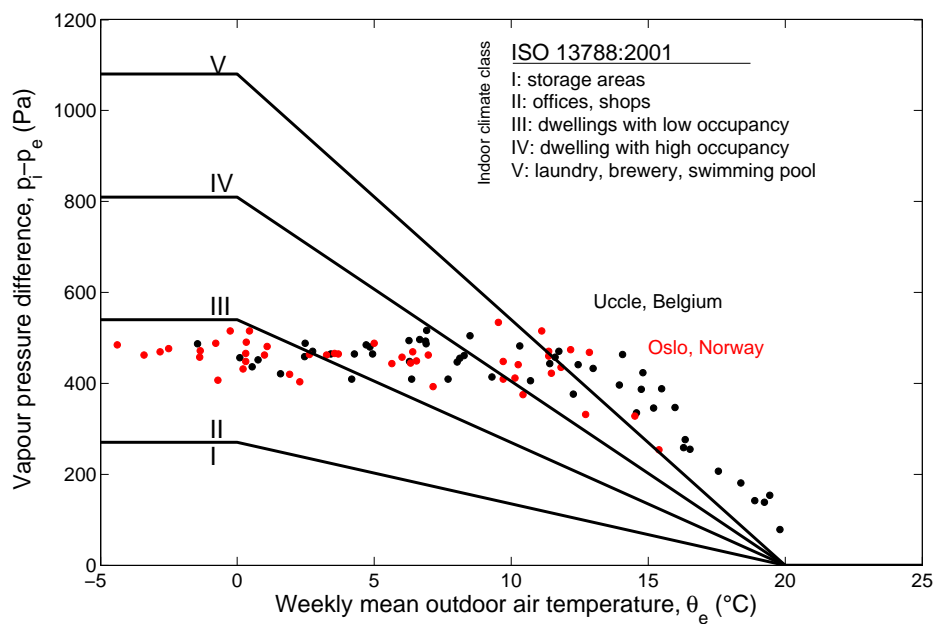


Figure 3: Vapour pressure difference between interior and exterior conditions for Uccle (Belgium) and Oslo (Norway).

This section gave a brief overview of the applied boundary conditions. For a more details on the applied climate conditions the reader is referred to Langmans (2013).

4 Simplifications of simulation grid

Although, DELPHIN 5 applies an efficient ODE-solver (Nicolai 2007) for the integration in time, yearly two-dimensional heat, air and moisture simulations within building components remain time consuming calculations. The simulation time for the general wall configuration, discussed in section 2.2 was approximately 7 hours (on a 3.07 GHz / 48 GB computer). As consequence, it becomes interesting to verify the impact of modelling simplifications to reduce these simulation times. This section studies the impact of two grid simplifications for the wall configuration of Figure 2a: (1) excluding top and bottom plate from the simulation grid and (2) excluding the service cavity from the simulation grid (the properties of the service cavity are in this case included in the transfer coefficients). Main emphasis is on the

justification and the corresponding simulation performance of the proposed modelling simplifications. The exterior air barrier in this reference simulations is BIFBa and the insulation material is MW20.

4.1 Grid sensitivity

Before modelling simplifications can be introduced, a reliable reference simulation grid needs to be defined first. Therefore, this section starts with a grid sensitivity analysis. Best simulation performance was obtained with an equidistant grid. Consequently, an equidistant 124 by 42 grid, depicted in Figure 2a, was selected. To verify the accuracy of this proposed grid, a sensitivity analysis was performed with a refinement factor of 1.5, resulting in a 186 by 63 equidistant grid. Figure 4 investigates the impact of this grid refinement for (a) the moisture content at the top of the exterior air barrier and (b) the ventilation rate behind the cladding. The results show that the obtained differences between these two grids are less than $\pm 5\%$ for both the moisture content levels and the ventilation rates. This is an acceptable error level, so, the proposed grid of Figure 2a will applied for the further simulations in this study.

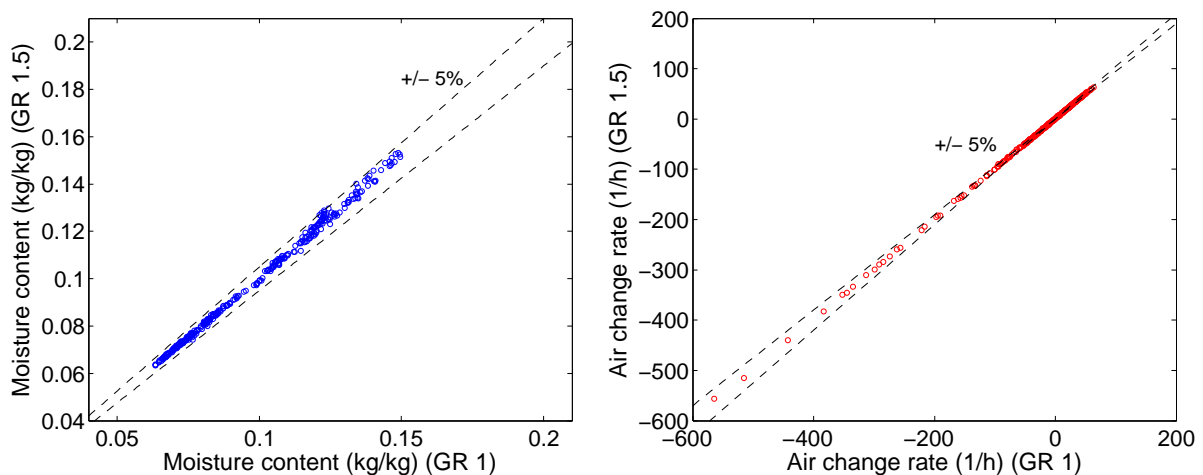


Figure 4: Impact of a grid refinement ($\times 1.5$) on (a) the top moisture content of the exterior air barrier and (b) the ventilation rate behind the cavity (daily averaged values).

4.2 Interior finishing materials

As the highest moisture levels are concentrated at the exterior of the building component, it can be questioned whether the inner service cavity and adjacent finishing layers should be modelled in detail (Figure 2b). To answer this question Figure 5a compares the moisture content of the exterior air barrier for the simulation including these layers and the simulation wherein these layers are incorporated in the interior heat and vapour transfer coefficients. Note that the air resistance of the service cavity and the inner finishing board are neglected in the latter approach. Figure 5a illustrates that the impact of this simplification is less than 5%. As a result, the inner service cavity and gypsum board can be safely modelled as transfer coefficients, corresponding to a 30% reduction of the simulation time.

4.3 Top and bottom plate

A third potential simplification in the simulation grid is the omission of the top and bottom plates. Commonly, these top and bottom plates are included in hygrothermal modelling of lightweight walls (e.g. Geving 1997, Økland 1998). For the current configuration, however, it was noticed that including the top plate did not increase the hygrothermal risk of the component. In contrast, it was observed that the moisture content level at the top of the exterior air barrier increased by excluding the wooden plates from the simulation grid.

This can be explained by a combination of the higher thermal conductivity and hygroscopic buffer capacity of the wood in comparison with the mineral wool. The first results in higher temperatures at top of the exterior air barrier, and thus, lower relative humidity levels when the plates are present. The latter reduces the moisture load on the exterior barrier as the incoming vapour flux can be partly stored in the wood. Figure 5(b) compares the moisture content at the top of the exterior air barrier for the simulation with and without top and bottom plates (in blue). In addition, also the moisture content of the exterior barrier just below the top plate is included in this comparison (in green). The figure illustrates that the highest moisture content is shifted downward by including the top plate in the calculation grid. Additional simulations in which the wooden plates were modelled with the same thermal conductivity as the mineral wool layer revealed that the hygroscopic buffer capacity of the wooden plates has the highest impact on the reduced moisture load on the exterior air barrier. Furthermore, the impact on the mould growth index was verified as well. For both the simulation with and without plates the maximum mould growth index equals 3.4 (-) and is located at 16-18 cm from the top of the wall. This is significantly higher than the most critical mould growth level obtained in the wooden plates, which was only 0.65 (-).

In summary, it can be concluded that excluding top and bottom plate from the simulation grid results in a slightly more critical situation. As a consequence it is a safe assumption to remove both plates from the simulation grid. By excluding the wooden plate from the grid the simulation time could be reduced by 25 %.

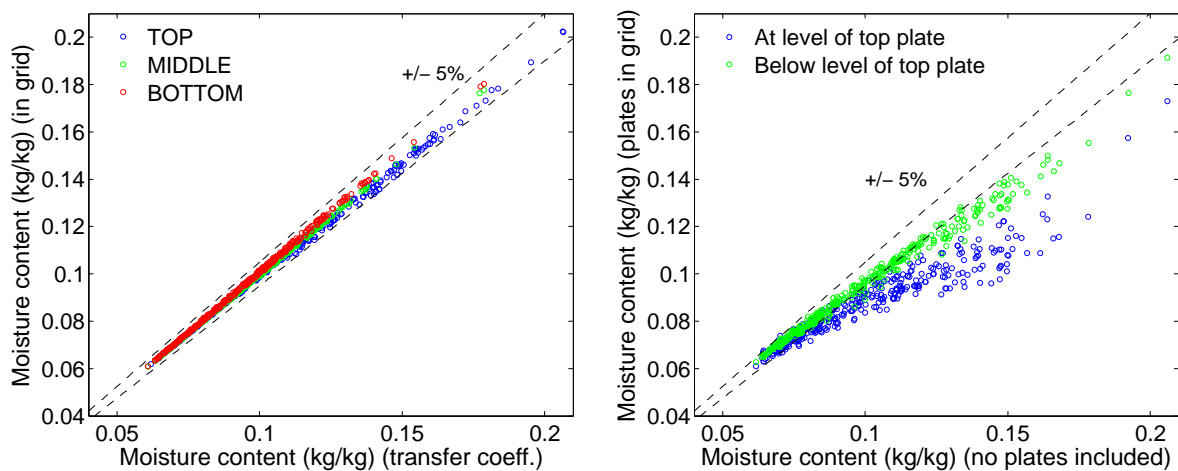


Figure 5: (a) Impact of introducing inner finishing layers as transfer coefficient and (b) simulation with and without wooden plates (daily-averaged values).

5 Parameter analysis and discussion

This section provides a parameter analysis on the global wall configuration discussed in section 2.2. First, the hygrothermal performance of two different commonly applied insulation materials is studied: (a) mineral (glass) wool and (b) loose-fill cellulose insulation. These simulations are performed with an BIFBa exterior air barrier. Thereafter, the performance of several other potential exterior air barrier materials, such as OSB, fibre cement board, foils and gypsum board, are investigated. Finally, several variants of the reference case are simulated under other European climate conditions, from Lisbon to Helsinki.

5.1 Insulation material

First, the impact of the insulation material is investigated. Two commonly applied groups of insulation materials are selected for the numerical investigation here: (1) mineral wool and (2) blown-in cellulose insulation. Most often glass wool insulation blankets with a density of 20 kg/m^3 (MW20) are used in Belgium. Densities of 30 kg/m^3 (MW30), which have a slightly better thermal resistance performance, have only a limited market as they are more expensive. Nevertheless, both densities (MW20 and MW30) are included in the investigation here. For blown-in loose-fill cellulose insulation densities of around 60 kg/m^3 , commonly applied in practice, are adopted here. In addition, cellulose insulation with lower densities (40 kg/m^3 and 50 kg/m^3) are examined as well. The air permeability levels for these lower densities are based on measurements of [Yarbrough & Wudhapitak \(1992\)](#) (see Table 2).

Table 2 presents the maximum mould index and accumulated condensation on the exterior air barrier for the reference configuration (Figure 2) for the discussed insulation materials. The predicted maximum mould index never exceeds the proposed limit of 3 and no condensation occurred for the wall elements insulated with cellulose. For the mineral wool insulation, however, mould growth problems are predicted for the standard density of 20 kg/m^3 . A mould index of 4.3 was found for this density, corresponding to a visual mould covering percentage between 10-50 %. Mineral wool with increased density (30 kg/m^3), in contrast, meets the proposed moisture limit state. Finally, this table shows that no condensation occurred for both the mineral wool and cellulose insulated walls.

	Cellulose			Mineral wool	
	40	50	60	20	30
$\rho \text{ (kg/m}^3\text{)}$					
$K_{\parallel} \text{ (m}^2\text{)}$	$2.8 \cdot 10^{-9}$	$1.4 \cdot 10^{-9}$	$8.8 \cdot 10^{-10}$	$5.3 \cdot 10^{-9}$	$3.2 \cdot 10^{-9}$
$K_{\perp} \text{ (m}^2\text{)}$	$2.8 \cdot 10^{-9}$	$1.4 \cdot 10^{-9}$	$8.8 \cdot 10^{-10}$	$1.7 \cdot 10^{-9}$	$8.1 \cdot 10^{-10}$
M (-) / AC_{max} (kg/m²)	2.3/-	1.8/-	1.6/-	4.3/-	2.3/-

Table 2: Maximum mould index (-) and accumulated condensate for different insulation materials and densities.

In addition, Table 2 provides the air permeability levels of the different insulation materials and densities. From this table it follows that higher air permeability levels correspond to a higher mould growth index. This can be explained by the increased amount of natural convection inside the component, resulting in a higher moisture ingress. Table

2 demonstrates that no moisture problems are expected for loose-fill cellulose insulated wall elements. Even for densities significantly lower than 60 kg/m^3 - rarely applied in practice - no problems occurred. In contrast, however, the simulations predicted critical mould levels for standard mineral wool insulation (MW20). From this table it can be concluded that applying high density mineral wool (30 kg/m^3), with a lower air permeability, is an effective measure in decreasing the moisture load. Yet it should be stressed that the results of Table 2 correspond to an 'ideal' installation of the insulation layer, in that, perfect contact between the insulation and the adjacent layers is assumed. Experimental results of Janssen (1997) and Brown et al. (1993) indicated that small air channels along glass wool batt insulation are unavoidable in practice, increasing the potential for natural convection. In order to produce realistic simulation results, the presence of small air cavities around mineral wool insulation are considered. The simulations with mineral wool insulated elements were repeated, introducing imperfections along the interface for the insulation and the adjacent layers. Herein, six configurations are investigated, varying the position of these air cavities: an air channel along the (a) cold sides of the insulation, (b) warm side of the insulation layer, (c) at the top of the insulation, (d) both cold and warm sides, (e) both the cold and warm side and at the top of the insulation, and (f) at all four sides of the insulation. For these configurations the impact of channels of 1 mm, 3 mm and 5 mm have been studied. All combinations are simulated for both mineral wool with a density of 20 kg/m^3 and 30 kg/m^3 for which the corresponding simulation results are summarised in Table 3.





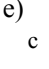
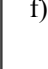
		Mineral wool											
		a) 		b) 		c) 		d) 		e) 		f) 	
cavity	density	20	30	20	30	20	30	20	30	20	30	20	30
	1 mm		4.5/-	2.8/-	4.4/-	2.5/-	4.5/-	2.9/-	4.6/-	3.7/-	4.8/-	4.1/-	4.8/-
3 mm		5.5/-	4.6/-	4.6/-	3.2/-	4.7/-	3.6/-	5.8/-	5.1/-	6/1.1	6/0.6	5.9/1.4	6/1.2
5 mm		5.9/-	4.9/-	4.8/-	4/-	4.7/-	3.7/-	6/0.1	5.6/-	6/>5	6/4.5	6/>5	6/>5

Table 3: Impact of air channels (1 mm, 3 mm and 5 mm) around insulation layer on the maximum Mould index (-) and maximum accumulated condensation (kg/m^2) for mineral wool with a density of 20 kg/m^3 and 30 kg/m^3 . The coloured lines indicate the position of the air channel (c:cold side / w:warm side).

This table confirms that the risk for moisture problems is highly influenced by the presence of small air channels along the mineral wool layer. Even a small air channel of 1 mm at both sides of the insulation (configuration d) increases the mould index from 2.3 to 3.7 for MW30. As a consequence, the above-mentioned hypothesis that higher mineral wool densities decrease the risk for moisture problems only holds for perfect contact conditions. From the moment imperfections around the mineral wool insulation layer (which definitely occur in practice) are considered, the density of the mineral wool becomes of minor importance.

Again, Table 3 shows that most critical moisture limit state corresponds to mould growth. Only for air channels of 3 mm and 5 mm on at least two side of the insulation condensation occurred. To illustrate the obtained condensation profiles. Figure 6 depicts on an hourly basis the accumulated condensation along the height of the exterior air barrier for MW20 with air channels of 5 mm at both sides (configuration d). This graph demonstrates that condensation

clearly occurs during winter periods and is concentrated at the upper height of this layer.

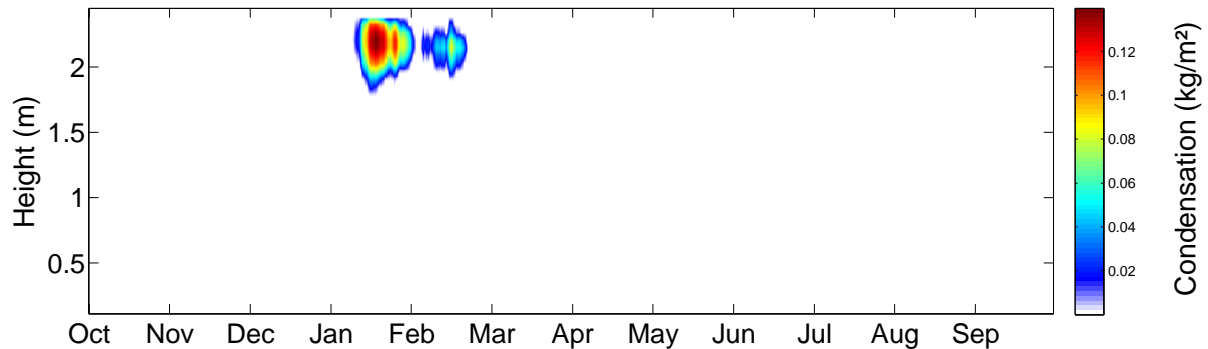


Figure 6: Accumulated condensation along the exterior air barrier for mineral wool of 20 kg/m^3 and air channels of 5 mm on both vertical sides of the insulation layer (based on hourly data).

5.2 Exterior air barrier material

Next, the impact of the exterior air barrier material is investigated. So far, all simulations were performed with bituminous impregnated wood fibreboards with an air resistive coating (BIFBa). This section examines the performance of other potential air barrier materials: (a) bituminous impregnated fibreboard without additional coating (BIFBb), (b) fibre cement board (FCB), (c) spunbonded foil (FOIL), (d) gypsum board (GB), (e) OSB, (f) BIFBb + FOIL, (g) GB + FOIL and (h) OSB + FOIL. These materials and their combinations are commonly applied as wind barrier in Belgium, except gypsum board which is rarely used at the exterior of the building envelope. Yet this material is included in the analysis, as it is frequently used as wind barrier in Norway. It should be noted that gypsum board applied for exterior applications is water resistant in contrast to its generally known variant used as interior finishing layer. The properties of these materials are documented in section 2.3. In addition to the very vapour permeable spunbonded foil ($\mu_{d,90} = 0.05 \text{ m}$), discussed in section 2.2 (FOIL), two variants with higher vapour resistances are included in the analysis here: FOIL01 and FOIL02, corresponding to a constant μ_d -value of 0.1 m and 0.2 m, respectively.

These potential air barrier materials are investigated for the reference configuration (section 2.2), insulated with mineral wool (MW30) and loose-fill cellulose insulation (CL60). In case of mineral wool, air channels of 3 mm are considered on both sides of the insulation layer.

Table 4 gives the overview of the simulated maximum mould growth index and the accumulated condensation. Here, results exceeding the proposed limit state (section 2.4) are indicated with a coloured background. The table confirms the above observation that the mineral wool insulated walls result in higher moisture loads compared to loose-fill cellulose insulation. For all except one of the walls with glass wool, critical mould levels are predicted. Only for gypsum board the simulated mould index is lower than the threshold of 3. When this gypsum board is however

combined with a spunbonded foil on the exterior side the risk for mould growth increases. Moreover, the combination of gypsum board covered with a foil results in an accumulated condensation amount of 0.53 kg/m^2 , exceeding the proposed limit state. Condensation is predicted for all configurations applying foils as exterior air barrier. The amounts for the foil with the highest vapour diffusion permeability (FOIL) are limited, passing the moisture limit state of 0.1 kg/m^2 . However, the foils with increased vapour diffusion resistance exceed this threshold value, resulting in run-off conditions.

	MW30		CL60		
	M_{\max}	AC_{\max}	M_{\max}	AC_{\max}	$MC_{\text{cel,max}}$
BIFBa	5.1	/	1.6	/	0.16
BIFBb	6	0.17	5.6	/	0.42
FCB	4.9	/	1.7	/	0.36
GB	1.2	/	0.4	/	0.16
OSB	4.4	/	1.4	/	0.20
GB+FOIL	3.8	0.53	0.6	/	0.17
BIFBb+FOIL	4.2	/	0.6	/	0.14
OSB + FOIL	4.5	/	1.4	/	0.18
FOIL	x	0.04	x	/	0.17
FOIL01	x	0.19	x	/	0.19
FOIL02	x	0.73	x	/	0.32

Table 4: Maximum mould index (-), Accumulated Condensation (kg/m^2) and Moisture Content of the cellulose insulation (kg/kg) for configurations with different exterior air barrier materials. (x=as the foil consist of non-organic material the mould index on these material is not verified).

For the wall elements insulated with loose-fill cellulose insulation, on the other hand, only moisture problems are predicted for the BIFBb air barrier materials ($M=5.6$). As discussed in section 2.3 this material is relatively air permeable which may result in forced convection conditions, and thus, substantial moisture loads. Nevertheless, the simulations do not predict condensation conditions for this configuration with cellulose insulation. Therefore, also the maximum moisture contents of the cellulose are included in the Table 4. The results show that the highest moisture content of the cellulose occurs for the wall with BIFBb (0.42 kg/kg). Yet, such values are close to conditions for which deformations of cellulose may occur (Derome 2005).

5.3 Different European Climates

Finally, the hygrothermal response of wall elements with an exterior air barrier is studied for various European climate conditions. The selected locations cover a wide range of European climates. Main focus, however, is on the Northern climates and particularly on Scandinavian regions. Recent building practice in Norway tends to focus on increasing the airtightness of the exterior layer, as stated by e.g. Myhre & Aurlien (2005), Holøs & Relander (2010). Therefore, special attention was given to this country by including Stavanger, Oslo, Bergen and Trondheim in the analysis. Figure 7 shows an overview of all locations studied. The corresponding climate files have been retrieved from the software package Meteonorm. In addition, Figure 7 compares the selected climates by means of averaged climate indicators.

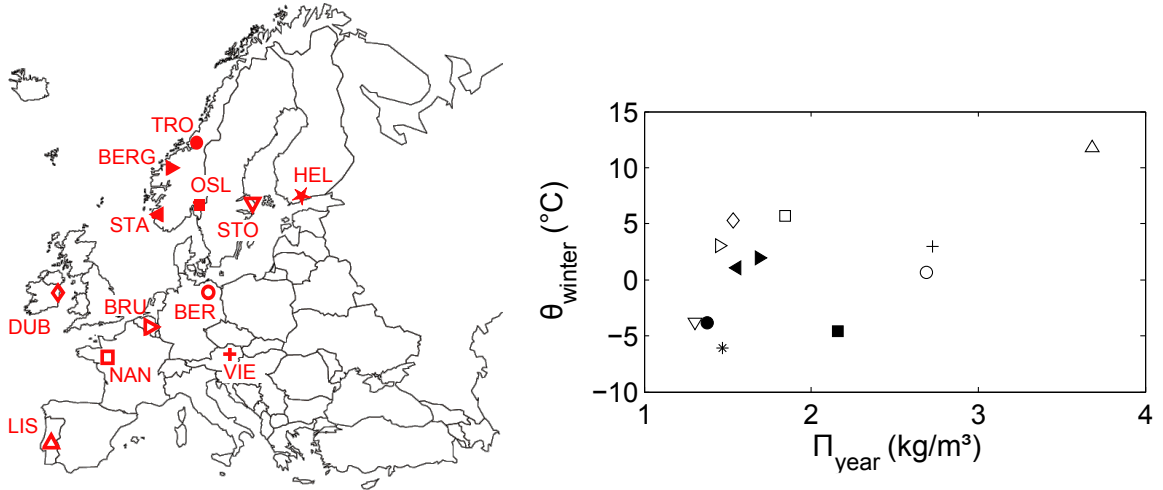


Figure 7: Overview of the European locations for which simulations are performed.

First, the averaged outdoor winter temperatures² (θ_{winter}), provides a direct indication of the level of buoyancy driven air flow within the insulation layer, and thus, the increased moisture loads. Second, the Π_y -factor expresses the severeness of the exterior climate. This factor (kg/m^3), proposed by [Hagentoft & Harderup \(1993\)](#) for the selection of reference years, calculates the yearly averaged difference between the vapour concentration in the outdoor air and the maximum moisture concentration on the building envelope surface on hourly data:

$$\Pi_y = \overline{v_{out,sat}(\theta_s) - v_{out}}_{year} \quad (2)$$

in which $v_{out,sat}(\theta_s)$ represents the saturation vapour concentration at the buildings surface for a North oriented wall and v_{out} corresponds to the moisture concentration of the outdoor air. As this value is calculated on a yearly basis, it represents the drying potential of the climate, and is thus, a relevant indicator for the severeness of the climate for the purpose of this study.

Both the averaged outdoor winter temperatures (θ_{winter}) and the Π_y -factor of the climates investigated are depicted in Figure 7. This graph illustrates how the Southern European climate, Lisbon, combines a high averaged winter temperature with a high Π_y -factor. Furthermore, this figure clearly shows higher Π_y -factors for Eastern European climates (Berlin, Vienna) compared to the Western European locations (Brussels, Nantes, Dublin). In contrast the Western European climates tested correspond to milder winter temperatures. Most critical locations expected are Helsinki, Stockholm and Trondheim, in that they combine low winter temperatures with low Π_y -factors. Furthermore, this graph illustrates great differences between the four Norwegian climates included.

The simulations are performed for the wall configuration discussed in section 4.1 for which either MW30 with two vertical channels of 3 mm on both sides or CL60 is applied. For the exterior air barrier material, on the other hand,

²average of December, January and February

two variants are included: (a) BIFBa and (b) FOIL (see section 2.3 for the corresponding material properties).

Figure 8 depicts the simulation results for the wall elements insulated with mineral wool. Here, the maximum mould growth index within the walls using BIFBa exterior air barriers are depicted on the top row and the maximum accumulated condensation amounts for the elements with a FOIL on the bottom row. These graphs contain the same information, however, the left hand side is given as a function of θ_{winter} and the right hand side is presented as a function of Π_y . Out of the 12 climates tested only the Eastern European (Berlin, Vienna), the Southern European (Lisbon) and two of the Northern European locations (Oslo, Bergen) result in mould growth levels lower than 3. From this figure it follows that Π_y is the most dominating climate parameter in the prediction of mould growth. For these limited number of climates it appears that no problematic mould growth is observed for Π_y -factors higher than 2 kg/m^3 . When it comes to condensation amounts on the non-hygroscopic foil (bottom row in Figure 8), however, it appears that the temperature is the dominating climate parameter. Here, only the coldest climates results in excessive condensation levels (Stockholm, Helsinki, Oslo and Trondheim). It should be stressed that the condensation levels for the coldest climates, Helsinki and Stockholm, even exceed the proposed threshold value of 0.1 kg/m^2 with one order of magnitude. The same simulations are repeated for wall elements insulated with cellulose insulation. The results are presented in a similar way in Figure 9. In contrast to the mineral wool insulated walls, no moisture problems are found for the wall elements simulated with loose-fill cellulose insulation. Because of the hygroscopic properties of this insulation material, no condensation occurs for these configurations. As a consequence the bottom row in Figure 9 depicts the

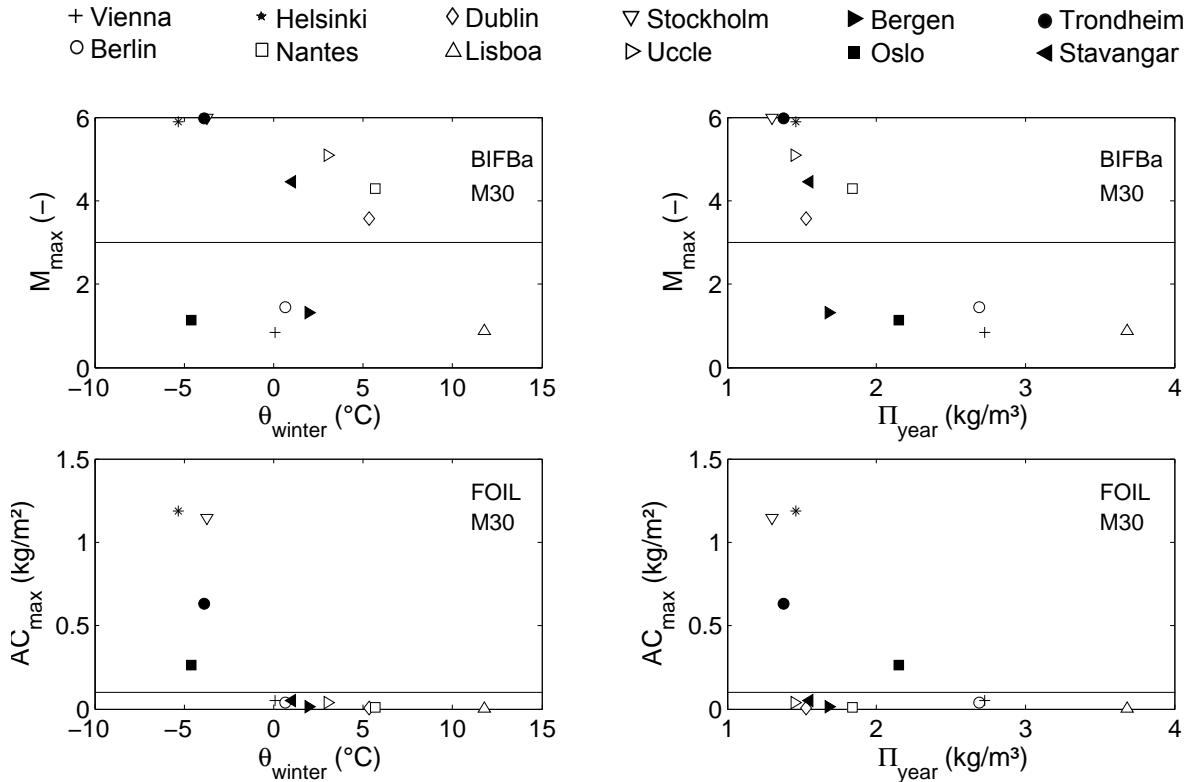


Figure 8: Performance of wall systems insulated with mineral wool (MW30) and either an exterior air barrier of BIFBa or FOIL: Top) maximum mould index on BIFBa. Bottom) accumulated condensation on FOIL.

highest moisture contents of the cellulose insulation instead. High moisture contents of cellulose insulation may result in deformation of the material which may influence its properties. The highest moisture levels of the cellulose insulation are found for Stockholm and Helsinki. Though, these levels are still below 0.3 kg/kg for which no deformation are expected (Langmans 2013).

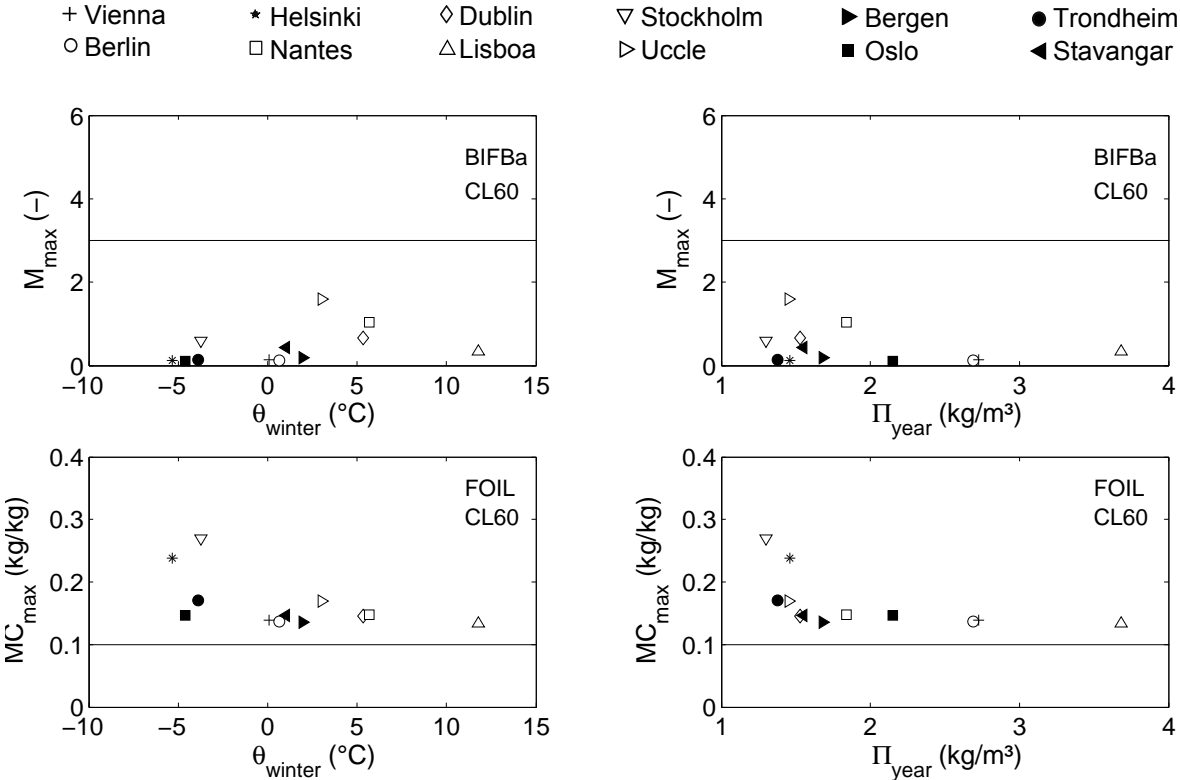


Figure 9: Performance of wall systems insulated with cellulose (CL60) and either an exterior air barrier of BIFBa or FOIL: Top) maximum mould index on BIFBa. Bottom) maximum moisture content of cellulose for walls with FOIL.

In summary, this section explored the hygrothermal response of highly insulated wall elements with an exterior air barrier in various European climates. In total 12 climates were verified, covering a range from North to South Europe. From this data it follows that Northern and Western Europe are most vulnerable to moisture problems when such wall systems are insulated with mineral wool. When these walls are insulated with loose-fill cellulose insulation, however, no moisture problems were obtained for the European climates tested.

6 Conclusions

The present paper performed numerical simulations to assess the hygrothermal response of timber frame elements with the most airtight layer at the outside of the building envelope under realistic climate conditions. The simulations correspond to the situation in which the wind barrier is sealed, so it serves as an exterior air barrier. The discontinuities in the interior vapour retarder, on the other hand, are assumed unsealed. As a consequence this layer does not serve as an interior air barrier. These yearly simulations have been conducted with an adjusted version of DELHPIN 5 (Langmans 2013), and were restricted to highly insulated wall elements only.

The simulation results identified a large impact of the applied insulation materials on the performance of these components. In summary, the simulation results indicate that the use of loose-fill cellulose insulation is more appropriate than mineral wool blankets for light weight components with an exterior air barrier. The main reason for this lies in the lower air permeance of loose-fill cellulose insulation. In addition, highly insulated walls with mineral wool blankets are more vulnerable to air layers at material interfaces. Such deficiencies greatly amplify the level of natural convection in winter conditions, and thus, the risk for moisture problems. Besides different insulation materials, various exterior air barriers have been studied as well. Most of the exterior barriers resulted, in combination with mineral wool, in excessive mould growth and/or interstitial condensation. Only for the most vapour open spunbonded foil and gypsum board no problems were found. Yet in combination with cellulose insulation, the majority of the exterior air barrier materials performed well. Finally, the performance of highly insulated walls with an exterior air barrier was verified in various European climates. From the limited amount of locations tested, it followed that Northern and Western Europe regions were most vulnerable to mould problems. No mould problems were found for the (drier) continental climates, such as Berlin and Vienna. For interstitial condensation on spunbonded foils, however, the decisive climate parameter appeared to be the winter temperatures. Excessive amounts of interstitial condensation were found for the coldest climates, such as Helsinki, Oslo, Trondheim and Stockholm.

Acknowledgment

Research funded by a Ph.D. grant (grant number 81153) of the Institute for the Promotion of Innovation through Science and Technology in Flanders (IWT-Vlaanderen).

References

- Aho, H., Vinha, J. & Korpi, M. (2008), Implementation of airtight constructions and joints in residential buildings, in '8th Nordic Building Physics Symposium', Copenhagen, Denmark.
- Black, C. D. (2006), Mould Resistance of Full Scale Wood Frame by, Master thesis, University of Waterloo, USA.
- Bories, S. (1987), Natural convection in porous media, in J. B. Corapcioglu & M.Y., eds, 'Advances in transport phenomena in porous media', Martinus Nijhoff, pp. 77–141.
- Brown, W. C., Bomberg, M. T., Ullett, J. M. & Rasmussen, J. (1993), 'Measured thermal resistance of frame walls with defects in the installation of mineral fibre insulation', *Journal of Building Physics* **16**(4), 318–339.
- Derome, D. (2005), 'Moisture accumulation in cellulose insulation caused by air leakage in flat wood frame roofs', *Journal of Thermal Envelope and Building Science* **28**(3), 269–287.

- Desta, T. Z., Langmans, J. & Roels, S. (2011), 'Experimental data set for validation of heat, air and moisture transport models of building envelopes', *Building and Environment* **46**(5), 1038–1046.
- Geving, S. (1997), Moisture design of building constructions: hygrothermal analysis using simulation models, PhD thesis, NTNU Trondheim.
- Grunewald, J. (1997), Diffusive and convective mass and energy transport in capillary porous building materials (in German), PhD thesis, University of Technology Dresden, Germany.
- Hagentoft, C. E. (1991), Forced and natural convection coupled with heat conduction in walls with air gaps, in 'Proceedings of the seventh international conference of Numerical methods in thermal problems', Stanford, USA.
- Hagentoft, C.-E. (2002), HAMSTAD: WP2: Benchmark package, Technical report, University of Technology, Chalmers, Gothenburg, Sweden.
- Hagentoft, C.-E. & Harderup, E. (1993), Reference years for moisture calculations, Technical report, T2-S-94/01, IEA Annex 24, HAMTIE and Lund University, Department of Building Physics, Report TVBH-7171.
- Hens, H. (2010), *Applied Building Physics: Boundary Conditions, Building Performance and Material Properties*, Ernst & Sohn Verlag GmbH (a John Wiley Company), Berlin, London, New York.
- Holøs, S. B. & Relander, T.-O. (2010), Airtightness Measurements of Wood Frame Low Energy Row Houses, in '2nd Building Enclosure Science and Technology conference', Portland, pp. 1–11.
- Hukka, a. & Viitanen, H. a. (1999), 'A mathematical model of mould growth on wooden material', *Wood Science and Technology* **33**(6), 475–485.
- Janssen, H. (1997), Thermal performance of highly insulated wood frame walls, Master thesis, Norwegian University of Science and Technology, Norway.
- Janssen, H. & Roels, S. (2009), 'Qualitative and quantitative assesment of interior moisture buffering by enclosures', *Energy and Buildings* **41**(4), 382–394.
- Janssens, A. (1998), Reliable control of interstitial condensation in lightweight roof systems: calculation and assesment methods, PhD thesis, Departement of Civil Engineering, KU Leuven, Belgium.
- Janssens, A. (2003), Hygrische studie koud dak met cellulose-isolatie, Technical report, Ugent, Ghent, Belgium.
- Janssens, A. & Hens, H. (2007), 'Effects of wind on the transmission heat loss in duo-pitched insulated roofs: A field study', *Energy and Buildings* **39**(9), 1047–1054.
- Jokisalo, J., Kurnitski, J., Korpi, M., Kalamees, T. & Vinha, J. (2009), 'Building leakage, infiltration, and energy performance analyses for Finnish detached houses', *Building and Environment* **44**(2), 377–387.
- Kalamees, T. (2007), 'Air tightness and air leakages of new lightweight single-family detached houses in Estonia', *Building and Environment* **42**(6), 2369–2377.
- Kohonen, R. (1984), 'Transient analysis of the thermal and moisture physical behaviour of building constructions', *Building and Environment* **19**(1), 1–11.
- Kronvall, J. (1980), Air flows in building components, PhD thesis, Lund institute of technology, Sweden.
- Langmans, J. (2013), Feasibility of exterior air barriers in light weight construction, Phd thesis, KU Leuven.
URL: <http://bwk.kuleuven.be/bwff/PhDs/phdLangmans>
- Langmans, J., Klein, R., De Paepe, M. & Roels, S. (2010), 'Potential of wind barriers to assure airtightness of wood-frame low energy constructions', *Energy and Buildings* **42**(12), 2376–2385.
- Langmans, J., Klein, R. & Roels, S. (2012), 'Hygrothermal risks of using exterior air barrier systems for highly insulated light weight walls: a laboratory investigation', *Building and Environment* **56**(10), 192–202.
- Langmans, J., Klein, R. & Roels, S. (2013), 'Numerical and experimental investigation of the hygrothermal response of timber frame walls with an exterior air barrier', *Journal of Building Physics* **36**(4), 375–397.
- Langmans, J., Nicolai, A., Klein, R. & Roels, S. (2012), 'A quasi-steady state implementation of air convection in a transient heat and moisture building component model', *Building and Environment* **58**(12), 208–218.
- Lecompte, J. (1989), The influence of natural convection on the thermal quality of insulated cavity walls constructions (in Dutch), PhD thesis, Departement of Civil Engineering, KU Leuven, Belgium.

- Li, Q., Rao, J. & Fazio, P. (2009), 'Development of HAM tool for building envelope analysis', *Building and Environment* **44**(5), 1065–1073.
- Myhre, L. & Aurlien, T. (2005), Measured airtightness in low-energy houses, in '7th Nordic Building Physics Symposium', Reykjavik, Iceland.
- Nicolai, A. (2007), Modelling and numerical simulation of salt transport and phase transitions in unsaturated porous building materials, PhD thesis, Syracuse University, USA.
- Nore, K. (2009), Hygrothermal performance of ventilated wooden cladding, PhD thesis, Norwegian University of science and technology, Norway.
- Økland, Ø. (1998), Convection in highly-insulated building structures, PhD thesis, Norwegian University of Science and Technology, Trondheim, Norway.
- Piecková, E. & Jesenská, Z. (1996), 'Microscopic fungi in dwellings and their health implications', *Ann Agric Environ Med* **6**(1).
- Reboux, G., Bellanger, A., Roussel, S., Grenouillet, F. & Millon, L. (2010), 'Moulds in dwellings: health risks and involved species (in french)', *Rev. Mal Respir.* **27**(2), 118–121.
- Roels, S., Talukdar, P., James, C. & Simonson, C. J. (2010), 'Reliability of material data measurements for hygroscopic buffering', *International Journal of Heat and Mass Transfer* **53**(23-24), 5355–5363.
- Saeid, N. H. & Pop, I. (2004), 'Transient free convection in a square cavity filled with a porous medium', *International Journal of Heat and Mass Transfer* **47**(8-9), 1917–1924.
- Sedlbauer, D. K. (2001), Prediction of mould growth on and in building components (in German), PhD thesis, University of Stuttgart, Germany.
- Silberstein, A. & Hens, H. (1996), 'Effects of air and moisture flows on the thermal performance of insulations in ventilated roofs and walls', *Journal of Building Physics* **19**(4), 367–385.
- Stranger, M., Verbeke, S., Verbeke, L., Geyskens, F., Swinnen, R., Goelen, E., Taubel, M., Hyvarien, A., Laverge, J., Janssens, A., Wuyts, D. & Ingelaere, B. (2012), Exploratory research on the quality of the indoor environment in energy efficient buildings: the influence of outdoor environment and ventilation, Technical report, VITO-LNE.
- Swami, M. & Chandra, S. (1987), Procedures for calculating natural ventilation airflow rates in buildings, Technical report, FSEC-CR-163-86, Florida Solar Energy Center, Cape Canaveral, Florida, USA.
- Tariku, F., Kumaran, K. & Fazio, P. (2010), 'Transient model for coupled heat, air and moisture transfer through multilayered porous media', *International Journal of Heat and Mass Transfer* **53**(15-16), 3035–3044.
- Tenwolde, A. & Rose, W. B. (1996), 'Moisture control strategies for the building envelope', *Journal of Building Physics* **19**(3), 206–214.
- Thue, J. V., Skogstad, H. B. & Homb, A. (1996), 'Wood frame walls in cold climate - vapour barrier requirements', *Journal of Building Physics* **20**(1), 63–75.
- Uvsløkk, S. (1996), 'The Importance of Wind Barriers for Insulated Timber Frame Constructions', *Journal of Building Physics* **20**(1), 40–62.
- Van den Brande, T., Blocken, B. & Roels, S. (2013), 'Rain water runoff from porous building facades: Implementation and application of a first-order runoff model coupled to a HAM model', *Building and Environment* **64**(0), 177–186. **URL:** <http://www.sciencedirect.com/science/article/pii/S0360132313000942>
- Vereecken, E. & Roels, S. (2012), 'Review of mould prediction models and their influence on mould risk evaluation', *Building and Environment* **51**, 296–310.
- Vereecken, E., Roels, S. & Janssen, H. (2011), 'In situ determination of the moisture buffer potential of room enclosures', *Journal of Building Physics* **34**(3), 223–246.
- Vinha, J. (2007), Hygrothermal performance of timber-framed external walls in Finnish climatic conditions: A method of determining a sufficient water vapour resistance of the internal lining of a wall assembly, PhD thesis, Tampere University, Finland.
- Weber, J. E. (1975), 'The boundary-layer regime for convection in a vertical porous layer', *International Journal of Heat and Mass Transfer* **18**(4), 569–573.

- Yarbrough, D. & Wudhapitak, S. (1992), Air permeability of loose-fill residential insulations, *in* '8th international conference on thermal insulation', Millbrae, California, pp. 8–14.
- Zillig, W. (2009), Moisture transport in wood using a multiscale approach, PhD thesis, Departement of Civil Engineering, KU Leuven, Belgium.